Melting Behavior of High-Temperature Polymers

F. J. Medellín-Rodríguez and P. J. Phillips*

Department of Materials Science and Engineering, University of Tennessee, Knoxville, Tennessee 37996-2000

J. S. Lin

Solid State Division, Oak Ridge National Laboratory, Oak Ridge, Tennessee 37831

Received August 8, 1995; Revised Manuscript Received July 29, 1996[⊗]

ABSTRACT: The melting behavior of three representative semirigid polymers, poly(aryl ether ether ketone), poly(ethylene terephthalate), and poly(ethylene naphthalenate), has been studied. Analysis of experimental results indicates that the melting process is morphologically the reverse of the isothermal crystallization process with respect to primary and secondary structural elements. On this basis, it is hypothesized that melting of all three polymers occurs in three distinct steps, assuming that spherulites are composed of dominant lamellae and subsidiary branches. The latter might have originated either from material rejected from the dominant lamellae or from noncrystalline molecular sections in the vicinity of the dominant lamellae. Experimental results emerging from differential scanning calorimetry, polarized optical microscopy, and small-angle X-ray scattering can be explained in terms of such a morphology, for which two possible models are suggested.

Introduction

The melting behavior of isothermally crystallized thermoplastic semicrystalline polymers has been one of the most heavily studied areas in the field of polymer science. In general terms, the melting mechanism, usually analyzed through differential scanning calorimetry (DSC), manifests itself as multiple melting endotherms.

From the reported results, a number of hypotheses offered to explain the melting behavior have emerged, largely based on the behavior of the endotherms. One of the earliest, and most generally accepted, is the recrystallization mechanism,[1] which is supported by the experimental fact that an increase in the DSC scanning rate generally decreases the melting point of isothermally crystallized samples. The opposite is observed at slower scanning rates, and this was argued to give more time for the original crystals to reorganize into either more perfect or thicker crystalline structures, i.e., those having higher melting points. Some other hypotheses for explaining melting behavior have also emerged in the recent past. They have involved viscoelastic thermal responses[2] and morphological features.[3−5] This last school of thought has received considerable support recently through the concurrent use of several experimental techniques, instead of using DSC alone.

Three representative high-temperature polymers with different crystallization characteristics were selected for the present study in order to analyze the melting behavior of semirigid macromolecules. They are poly(aryl ether ether ketone) (PEEK), poly(ethylene terephthalate) (PET), and poly(ethylene naphthalenate) (PEN). The recrystallization hypothesis has been proposed for all of them,[6−15] and even calculations of parameters such as the equilibrium melting temperature have been determined on the basis of such ideas.[7]

A different view, particularly for studies of PEEK, has argued a possible relationship between melting endotherms and secondary crystalline structures.[3−5] In this context, our previously reported optical observations of the processes of crystallization and melting of PEEK, PEN, and PET[3] first indicated that phenomenologically the processes of crystallization and melting were morphologically reversed. It was so determined that "portions" of secondarily crystallized material would appear in melting endotherms in the reverse consecutive manner to those in which they were formed under isothermal crystallization conditions.

In the light of previous ideas, the work reported herein was designed with the purpose of systematically analyzing the melting behavior of these high-temperature polymers through isothermal crystallization, fast quenching, then reheating, and fast quenching again of samples with different thermal history. This was made in order to investigate the possibility of common morphological crystallization and melting mechanisms of semirigid polymers.

Experimental Section

Materials. Samples for this work were obtained from different sources. PEEK grade Victrex 450fp was kindly donated by ICI America. The weight-average molecular weight ($\bar{M}_w$) measured through gel permeation chromatography (GPC) was $M_w = 40\,000$. As such, this postreactor powder is not expected to contain after-synthesis additives.

PET was obtained from Eastman Chemical and was grade 10388. The intrinsic viscosity of this homopolymer was 0.90, corresponding to a number-average molecular weight $M_n = 22\,609$ and to a $M_w = 72\,860$ determined through GPC. The degree of polydispersity was 3.22.

PEN was donated by Prof. G. Zachmann of the Institut für Technische und Makromolekulare Chemie, Hamburg, FRG. The number-average molecular weight of the greenish coarse powder was $\bar{M}_n = 24\,000$, which was also determined through GPC.

Specimen Preparation. Thick 1-cm^2 samples of average thickness 0.70 cm of PEEK, PEN, and PET were prepared using stainless-steel frames. These frames were designed to fit into a Mettler FP84HT hot stage in order to obtain three portions of the same thermally treated sample. The first portions were directly characterized after isothermal crystallization from the melt and fast quenching to ice−water. The two remaining portions were also quenched to ice−water and then thermally scanned to critical temperatures at the same heating rate that had been used in the DSC. This was done to reproduce the crystallization process that occurred during

[⊗] Abstract published in *Advance ACS Abstracts,* October 1, 1996.

S0024-9297(95)01165-X CCC: $12.00

heating at 10 °C/min and then to "freeze-in" the structure generated by fast quenching to ice−water at 5 °C, so that ambient temperature characterizations could be carried out. All specimens were vacuum dried at 90 °C for 3 h before any new thermal treatment or experimental characterization was begun.

Differential Scanning Calorimetry. A Perkin-Elmer calorimeter DSC-7 was indium−lead calibrated before the PEEK scans and indium calibrated in the case of PEN and PET. A baseline was run before and after each calibration. All DSC scans were made at 10 °C/min and the sample chamber remained always under a constant flux of nitrogen at 0.5 L/min.

Wide-Angle X-ray Diffraction (WAXD). A portion of the isothermally crystallized sample was analyzed using WAXD in the transmission mode. A Rigaku Denki diffractometer was used with 30 mA for the intensity of the filament and an accelerating voltage of 40 kV. WAXD was used for identification and evolution of crystalline structures through comparison with the reported positions of the diffracting planes.

Optical Microscopy. Polarized optical microscopy (POM) was used in order to register the in situ behavior of thin films or glass-deposited samples with thermal treatments similar to those used in DSC, WAXD, and small-angle X-ray scattering (SAXS). A Mettler FP82HT hot stage was attached to an Olympus microscope, and a trinocular was used to photoregister the thermal evolution of the sample at the same time that observations were made and the amount of polarized light was measured. As in all DSC scans, the heating rate was always set at 10 °C/min under a flux on nitrogen of 0.5 L/min.

Small-Angle X-ray Scattering. The third portions of the samples were studied using SAXS. Experiments were carried out using the 10-m SAXS camera at the Center for Small Angle Research at the Oak Ridge National Laboratory, Oak Ridge TN. This instrument[16] uses Cu Kα radiation ($\lambda = 1.54$ Å) and a 20 × 20 cm^2 position-sensitive detector with elements ∼3 mm apart. It was used with a sample-to-detector distance of 2.176 m. The scattering intensity was stored in a 64 × 64 array. Corrections were made for instrumental background and detector efficiency (via an Fe^{55} radioactive standard which emits γ-rays isotropically) on a cell-by-cell basis. The data were radially averaged and converted to an absolute differential cross section by means of precalibrated secondary standards.[17] Absolute intensity is in reciprocal centimeter units.

Analysis of SAXS Data

The SAXS data were numerically reprocessed in order to relate the scattering to the crystal morphology. Several corrections were applied before calculations of the one-dimensional correlation function of the electron density fluctuations within the sample[18] could be carried out.

First, raw SAXS data were extrapolated using a four-data sequence which rendered a curvelike adjustment for $I(q)$ from low values of the scattering vector to $q = 0$. The Debye−Bueche model given by $I(q) = A/(1 + \xi^2 q^2)$, where A is a constant and ξ is an inhomogeneity length, has been reported as a good approach for this extrapolation. Some other options have included linear or polynomial extrapolations of this part of the curve.

As is commonly the case, under our experimental conditions we obtained only a small number of data points at low q values. Therefore, after applying the Debye−Bueche model, excessively high values of the intensity at $q = 0$ were sometimes obtained. In a typical example, the ratio between the I_o of the Debye−Bueche model and the I_o used here was as high as 250. To generate the needed scattering curve at low q, the value of I_o was first fixed at double the maximum intensity of the peak observed in each scattering experiment. In this form the I_o values ranged only between 30 and 10 cm^{-1} of absolute scattering intensity. For the rest of the needed scattering data, the q values were fixed at constant distance intervals of 0.25, 0.50 and 0.75 times the distance between the origin and the first minimum of the decay scattering function. The I values were obtained by multiplying the fixed I_o by 0.25, 0.50, and 0.75. In this form, the process generated a smooth decay curve from I_o. Linear extrapolations had little effect on the shape of the one-dimensional correlation function (see later), whereas polynomial extrapolations created differences in both the shape of the curve and the extrapolated value of $I(q)$ at $q = 0$. Therefore, we chose to use the aforementioned four-point curve method because of better consistency.

Second, the SAXS data were polynomially smoothed over the q range and then, in a third overall adjustment of data, "background" corrections were made. The latter are considered positive deviations from Porod's law[19] and may be associated with thermal motion, local disorder, or the onset of the wide-angle scattering region. When scattering data in the wide-angle region are not available, such as in the present work, the background scattering intensity can be considered constant[20] and the scattering intensity can be expressed as

$$I(q)\, q^4 = KpH^2(q) + I_{fl} q^4 \tag{1}$$

in accordance with eq 1, by plotting the smoothed data $I(q)q^4$ vs q^4. The slope of the expected straight line gives the constant background scattering intensity I_{fl}.

In a last correction to the SAXS data a sigmoidal-gradient interface model was introduced to correct Porod's law[19,20] and was applied to the tail of the scattering data in reciprocal space at high q values in accordance with

$$I(q)|_{q\to\infty} = Kp \exp(-\sigma^2 q^2)/q^4 \tag{2}$$

where σ^2 is the variance of the density transition of a Gaussian smoothing function and Kp is Porod's constant. Corrected intensities were so obtained and corrected data, I_{BPC}, vs q were used in order to obtain the one-dimensional correlation function of the electron density fluctuations perpendicular to the main face of a stack of crystals[18]

$$\gamma_1(r)_{BPC} = \frac{\int_0^\infty q^2 I_{BPC}(q) \cos(2\pi q r)\, dq}{\int_0^\infty q^2 I_{BPC}(q)\, dq} \tag{3}$$

The one-dimensional correlation function approach was originally designed for homogeneous ideal two-phase systems where a series of triangles centered at $r = 0$, L, $2L$, etc., reflect correlations within one lamella, next neighbors, second neighbors, etc. At $r = 0$, there is the formation of a medium triangle or the so-called "self-correlation triangle" and there is also the origin of a horizontal line that passes along the bases of the rest of the triangles which is called the "baseline". The negative absissa that gives place to the origin of the baseline is related to the volume sample crystallinity. In real systems, however, the baseline sometimes does not show up and it is necessary to obtain, with experimental data emerging from another technique, the volume fraction crystallinity that is needed to calculate the characteristic length. This last parameter could be either the crystalline or the amorphous portion within lamellar stacks. However, the low crystallinity levels used here increase the probability that it is the lamellar thickness. On the other hand, in this work it was

experimentally observed that a clear ultimate birefringent spherulitic crystal was recovered in every case just before the final melting point. This was an indication that at such a temperature most of the secondarily crystallized material had been melted and as a consequence there should be an increase of the amorphous portion within lamellar stacks. The SAXS characteristic length, however, did not increase much after such a melting process, but there was a large increase in long periodicity. This was as an indication that the strong change was related to the amorphous phase.

The baseline for the range of crystallinities considered here was not observed; therefore, the volume fraction crystallinity of our samples was determined using DSC.[21] The overall DSC crystallinity must be the summation of crystallinities both within spherulites (intraspherulitic) and between spherulites (interspherulitic). In the present study, however, we also purposely selected low levels of crystallinity in specimens having impinged spherulites. This decreases as a consequence the probability of having both high interspherulitic and intraspherulitic crystallization. Under our crystallization conditions, we also observed that most of the quiescent material was immediately crystallized in impinging superstructures in PEEK, PET, and PEN. Therefore, intraspherulitic crystallization was considered the highest probability in crystallizing this group of macromolecules. We also need to mention in advance that secondary crystallization was found to be related to the second DSC melting endotherm, its nature being assigned to subsidiary lamellae. The third melting endotherm was, on the other hand, associated with dominant lamellae, i.e., "mother" lamellar stacks. In the light of these concepts, crystallization conditions for our initial samples were selected to show a third melting endotherm, i.e., low levels of subsidiary lamellae in every case. In this way, the DSC overall crystallinity was considered associated with mother lamellar stacks rather than with other types of crystallinity.

Interfacial thicknesses were calculated by three different methods in order to compare results. A first method involved the sigmoidal-gradient interface model which was used to correct Porod's law[19] after background subtraction or

$$\ln[I(q)q^4 - I_{fl}(q)q^4] = \ln Kp - \sigma^2 q^2 \tag{4}$$

In accordance with eq 4, the slope of the expected straight line will give the variance σ^2 from whence the interfacial thickness E[22] can be evaluated from

$$E = \sqrt{2\pi}\sigma \tag{5}$$

For a second method, Vonk[23] assumed a linear electron density gradient across the interface whose smoothing function was a top-hat function of width E with an expanded Fourier transform of the autocorrelation of the smoothing function given in terms of q[19] by

$$H^2(q) = (1 - E^2q^2/12) \tag{6}$$

therefore the corrected Porod's intensity becomes

$$I(q)q^4 = Kp - \frac{KpE^2}{12}q^2 \tag{7}$$

Equation 7 represents a straight line whose slope contains the interface thickness E.

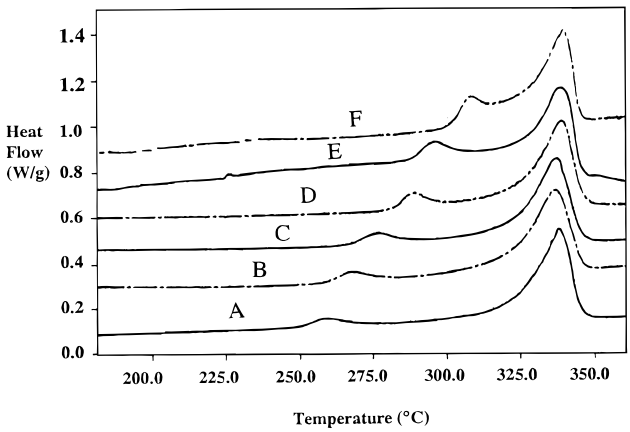

Figure 1. DSC melting behavior of PEEK after isothermal crystallization (1 h) from the melt (390 °C, 3 min): (A) 250, (B) 260, (C) 270, (D) 280, (E) 290, and (F) 300 °C.

For a third method, Ruland[20] used the sigmoidal model and expanded the Fourier transform of the smoothing function and obtained

$$I_{obs}(q)q^4 = 8\frac{k\pi}{lp} - \frac{8\pi k\sigma_z^2}{lp}q^2 \tag{8}$$

where k is the total scattered intensity (invariant) which is given by

$$k = \frac{1}{2\pi^2}\int_0^\infty q^2 I(q)\,dq \tag{9}$$

The variance σ_z^2 can be obtained from the slope of the straight line given by eq 8, and the interfacial thickness can be evaluated[22] through

$$d_z = \sqrt{2\pi}\sigma_z \tag{10}$$

Once the value of the interface thickness is obtained, the number-average lamellar thickness can be directly obtained from the plot of the one-dimensional correlation function and for example[21]

$$\langle T_c\rangle n = OQ + \frac{E}{3}\frac{\varphi}{1-\varphi} \tag{11}$$

where OQ is the distance from $r = 0$ to the interception of the tangent of the first decay and the baseline, E is the interface thickness, and φ is the volume fraction crystallinity.

Results

General Observations for PEEK, PEN, and PET. The melting behavior of isothermally crystallized PEEK, PEN and PET is shown in Figures 1, 2, and 3, respectively. The triple melting behavior of PET is clearly present from intermediate crystallization temperatures up to ~220 °C. As a generality, the behavior changes from two to three then two and finally one melting endotherm as crystallization temperature is increased. Similar results for PET were published by Zhou and Clough.[14] Our previous report[3] is the only published report of results for PEN. However, the DSC melting behavior of PEN is quite similar to PET, as shown in Figures 2 and 3. Triple melting behavior has not been reported for PEEK. However, Cheng et al.[9] proposed that the double melting traces observed in DSC could develop through the formation of a third intermediate, almost imperceptible, melting endotherm usually ob-

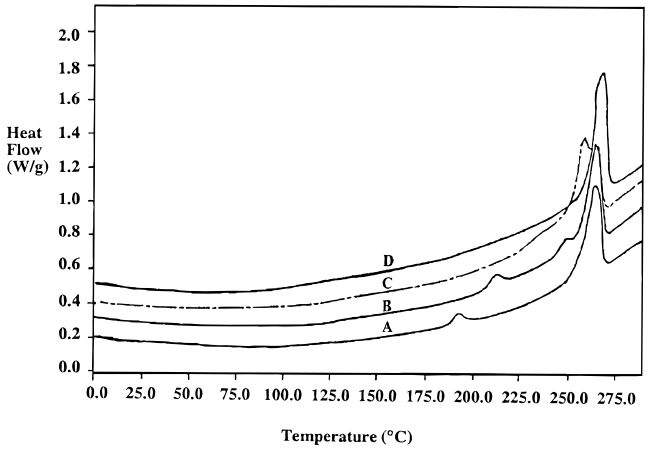

Figure 2. DSC traces of PEN after isothermal crystallization (2 h) from the melt (290 °C, 3 min): (A) 180 (α), (B) 200, (C) 220, and (D) 240 °C (*β*).

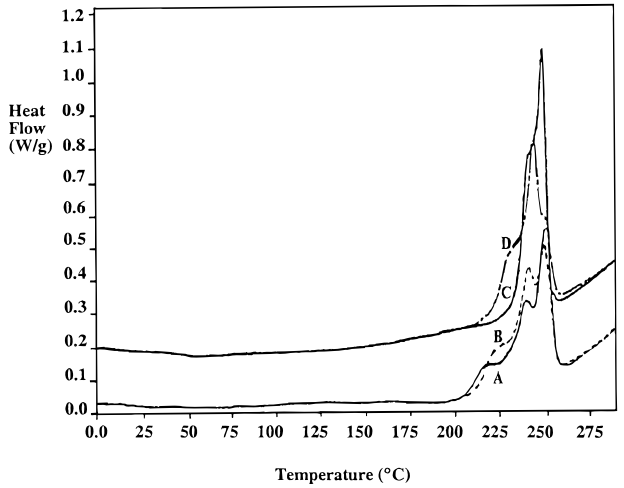

Figure 3. DSC traces of PET isothermally crystallized (2 h) from the melt (290 °C, 3 min): (A) 200, (B) 205, (C) 210, and (D) 220 °C.

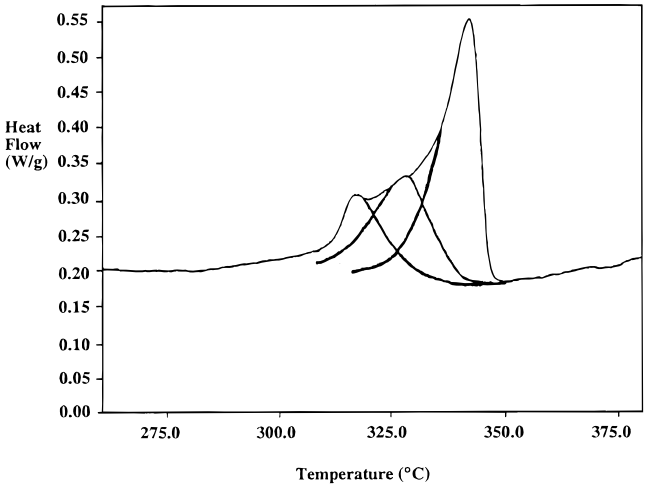

Figure 4. "Triple" melting behavior of PEEK isothermally crystallized from the melt (390 °C, 3 min): T_c = 310 °C; 10 min.

served at very low crystallization times. We conducted several experiments under different conditions; however, the triple melting behavior of PEEK could be verified only for very short crystallization times, as shown in Figure 4.

Optical microscopy first indicated that the processes of melting in all three polymers were morphologically

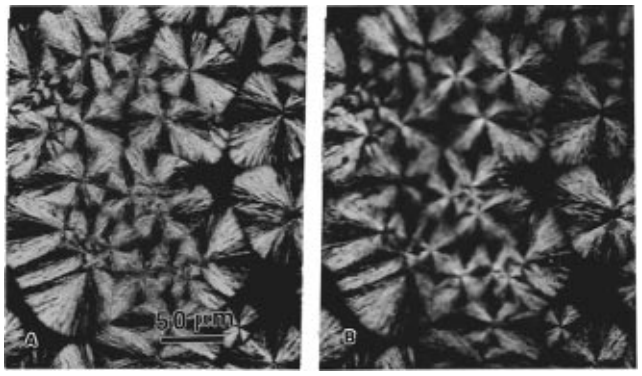

Figure 5. Typical micrographs of the melting behavior of PEEK after isothermal crystallization from the melt (390 °C; 3 min) at T_c = 310 °C: (a) prior to melting; (b) following melting of the secondary growth and prior to final melting of the spherulites.

the reverse of the sequence of crystallization. It is not meant to imply that the spherulites melt radially inward, but that the secondary growth within the spherulites disappeared first followed by the melting of the spherulites themselves in a conventional manner. Retardation inside spherulites was observed to appear on crystallization and disappear on melting in a steplike manner. Effects in PEEK were the weakest; therefore, analyses concentrated on this polymer. A typical melting process in PEEK is shown in the micrographs of Figure 5, where it is seen that secondary crystals melt first in a manner that is the reverse of their formation. The final stage of melting of PEEK involves the regeneration of a clear negatively birefringent spherulite, which ultimately melts as a whole.

Optical studies of melting in PET and PEN show that the phenomenon is similar to that of PEEK; however, a much higher proportion of secondary crystallization was observed, particularly in the case of PET. This behavior correlates relatively well with the proportion of the second melting endotherm observed in DSC traces shown in Figures 2 and 3. Optical studies of PET and PEN under conditions where there was only one melting endotherm present (at crystallization temperatures near the final melting point) did not indicate any specific melting sequence, the melting of primary and secondary crystals being superposed. This phenomenon was recently correlated with thermal mechanical analysis (TMA)[24] using PEEK. The behavior was taken as an indication that in this polymer the average melting point of secondarily crystallized material was very close to the melting point of the primary crystals. These characteristics would give rise to the appearance of double rather than triple melting behavior. It should also be noted that the regenerated ultimate spherulites of PET were positively birefringent and those of PEN negatively birefringent.

Specific Studies of PEEK. The change of depolarized light intensity during melting was measured in order to look for possible (microscopically undetectable) triple melting behavior. Typical results shown in Figure 6 clearly indicate the presence of three main thermal transitions on the basis of the changes of slope. It can also be seen that there was not a sharp thermal transition at the second melting endotherm, but a relatively broad and continuous process, unlike the one seen in the first endotherm.

There are no published reports of changes in the crystalline structure of PET and PEEK as a function of the degree of supercooling, unlike PEN, where a change from α to *β* crystalline structures was determined by

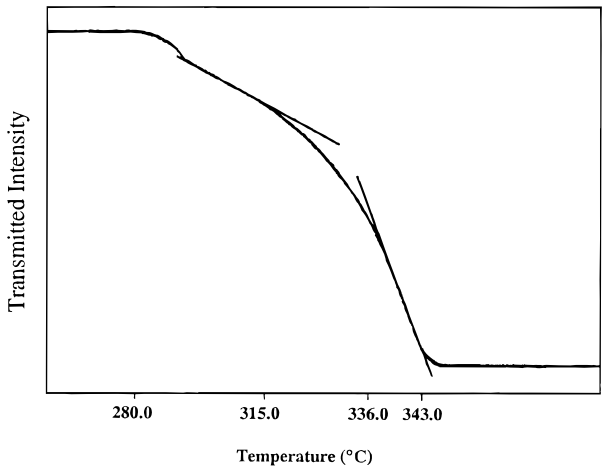

Figure 6. Total transmitted depolarized light intensity in an experiment heating from the crystallization temperature (280 °C) of PEEK after isothermal crystallization from the melt (390 °C, 3 min).

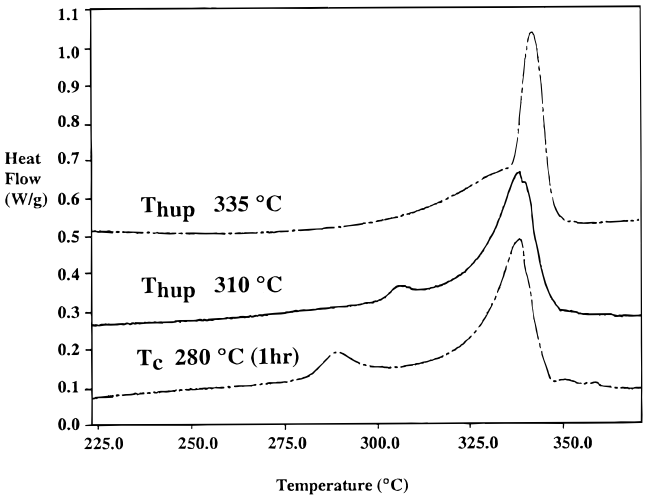

Figure 7. DSC traces of the systematic melting of PEEK. Crystallization from T_m = 390 °C, 3 min, and heating temperatures before quenching are shown.

Table 1. Treatment Temperatures and DSC Crystallinities of Samples Used for the Systematic Melting of PEEK, PEN, and PET

polymer	T_c (°C)	$T_{heat\ up}$ (°C)	$\%\chi_{DSC}$
PEEK	280 (1 h)		30.9
		310	30.5
		335	29.9
PEN	210 (0.5 h)		44.2
		240	42.4
		260	40.5
PET	200 (0.5 h)		28.0
		220	28.4
		247	29.2

WAXD and found to be dependent on the crystallization temperature in PEN.[15] In comparing the DSC traces of PEN and PET in Figures 2 and 3, however, quite similar triple melting behavior is observed in both cases despite the change in crystalline structure with crystallization temperature in PEN.

At this stage, as a generality, triple melting behavior was hypothesized to be reflective of a process in which material rejected from the primary lamellae was converted to secondarily crystallized material. The latter material would melt first, but mainly at the second melting endotherm in a steplike manner. These concepts mainly emerged from optical observations that indicated melting of secondary structures in thick regions of spherulites at the first endotherm, followed by melting of a higher amount of secondary structures near to the temperature at which the neat ultimate spherulite was regenerated. The latter finally disappeared at the third melting endotherm.

In an attempt to verify the conclusions reached from the microscopy experiments, some DSC studies were conducted on quenched material, processed in such a way as to simulate the melting sequence. As mentioned before, samples of each as-received polymer were isothermally crystallized and then quickly quenched in ice−water. Portions of each sample were heated at 10 °C/min to temperatures immediately above the first melting endotherm. Other portions were heated to temperatures immediately above the second melting endotherm for conditions under which triple melting behavior had been observed. In the case of PEEK, a hypothetical temperature of 10 °C below the final melting point was used as a reference to "eliminate" the unobservable second melting endotherm. Thermally treated samples of each polymer were then quickly quenched in ice−water before DSC, WAXD, and SAXS characterization.

The DSC traces of the treated PEEK are shown in Figure 7. The double melting behavior is clear and similar to reports in publications by other authors.[6−9] It can, however, be seen that after heating the sample up to a temperature immediately above the first melting endotherm, the endotherm disappeared and now a very small peak appeared at the temperature at which the linear heating was stopped. Even though not proven in the present study, it can be considered that this second small peak corresponds to new isothermal and instantaneously generated crystals of the quiescent polymer that had not crystallized earlier. The previous result combined with optical observations of PEEK involving the disappearance of some high-order colors (mostly green) give the first confirmation of steplike melting at the first melting endotherm.

After the sample was heated to 10 °C below the final melting point, the most noticeable feature of the PEEK DSC traces (see Figure 7) was the presence of a melting hump and a decrease of the total amount of the DSC crystallinity as shown in Table 1. In addition, the melting point of the main peak was slightly displaced to higher temperatures, presumably an indication of melting and reorganization of some kind to more perfect crystalline forms. Optical observations at this stage indicated the disappearance of all high-order colors and hence of secondary crystallization inside spherulites.[25]

WAXD patterns corresponding to the thermally scanned samples are shown in Figure 8. They did not show any significant change through the different stages of heating other than a decrease in crystallinity, which was expected for steplike melting.

The SAXS results provided very important correlative data. One-dimensional correlation function results for the thermal sequence of the PEEK samples are shown in Figure 9. At this point, it needs to be mentioned that in analyzing results it was optically verified that the process of fast quenching "froze-in" the morphology in every quenching step. From the results in Figure 9, it can be seen that after the first melting endotherm there is a slight recrystallization since the average lamellar thickness increases as indicated by the slope of the initial decay[22] and also a corresponding slightly higher increase in the long periodicity (position of the first maximum) (see also Table 2). As the heating temperature was increased to ∼10 °C below the final melting

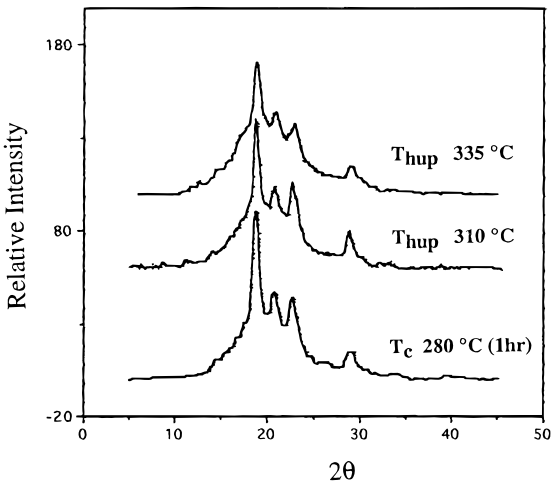

Figure 8. WAXD patterns for the systematic melting of PEEK.

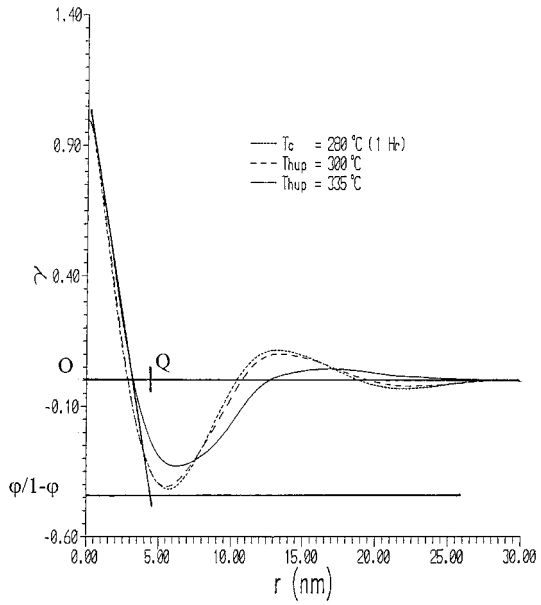

Figure 9. One-dimensional correlation function of the systematic melting of PEEK. Thermal conditions are shown together with the calculation of the distance OQ.

temperature there was still some recrystallization which, however, does not correspond to the large increase observed in the long periodicity.

Specific Studies of PET. The melting behavior of PET was quite similar to that of PEEK. However, correlating with the clear formation of a second melting endotherm in the PET DSC traces (Figure 10), the disappearance of secondary crystals was found to be much more pronounced optically.[25] If the secondary branching hypothesis is to be applied to PET, then larger increases in recrystallization and a long period should be expected since there is a higher second melting endotherm presumably related to such species. This expectation is seen to be verified in the SAXS results of Figure 11 where there is an increase of about 70% in the long period (see Table 2). An additional characteristic of the melting behavior of PET was the positive sign of the ultimate clear spherulites which, as in the case of PEEK, were also finally regenerated. This was taken as an indication of the nonselective evolution of the processes of crystallization and melting, which in spite of the orientation of the macromolecules was able to generate secondary crystalline structures. Other than a decrease in crystallinity, WAXD patterns of PET under melting conditions did not show any changes (Figure 12).

Specific Studies of PEN. Replacement by a naphthalene ring of the phenylene ring in the chemical structure of PET in order to form PEN creates a number of changes in the crystallization behavior. It was mentioned earlier that PEN is able to crystallize into two different crystalline structures.[15] As in PET, we have also noticed two different morphologies as a function of the degree of supercooling.[25] Formation of either triclinic α or triclinic β crystalline structures depends on the conditions of melting and crystallization. Melting (300 °C; 3 min) and crystallization (210 °C) temperatures chosen for this particular experiment correspond exactly to the transition point between the α and β crystalline structures,[15] i.e., a strongly metastable situation.

Figure 13 shows the DSC results for simulated melting of PEN. It can be seen that, after the crystallization period, three melting endotherms are present, as with PET. Another characteristic is a small crystallization exotherm just before the ultimate melting transition. After the PEN sample was heated to 240 °C (immediately above the first melting endotherm), other than the generation of a new small peak, the DSC traces were essentially unchanged. However, after the sample was heated to temperatures immediately above the second melting endotherm, a single melting peak (without the small exotherm) with higher melting point was again observed.

The WAXD patterns shown in Figure 14 did show a change in crystalline structure from α to β. Changes of this type were not observed in earlier studies[15] possibly because highly metastable conditions were used. At this point, there remains the need for an explanation of the process of melting of PEN. We invoke again the secondary crystalline structures to explain the results of the SAXS one-dimensional correlation function shown in Figure 15. Once again it can be seen that after the first melting endotherm there is a partial process of recrystallization, probably originating from melting of very thin crystals. Remains of such crystals could then be trapped by the main crystals in good agreement with the small increase in long periodicity shown through the first maximum of Figure 15 and Table 2.

After the sample was heated to temperatures close to the ultimate melting point, there was a strong recrystallization of PEN which on average increased in proportion to the lamellar thickness. The evolution of the recrystallization process may be related to the small exotherm observed in the DSC traces of Figure 2. The second melting endotherm of PEN is smaller than in PET (see the proportion of both second melting endotherms in PET and PEEK in Figures 1 and 3). Optical observations indicate a lower proportion of secondary effects disappearing on melting of PEN compared to PET (but higher than with PEEK). Therefore, the displacement of the long period of PEN in Figure 15 was expected to be intermediate between that of PEEK and PET. This was experimentally verified, and the results are shown in Table 2. In summary, in spite of the change of crystal structure, PEN also conforms to the triple melting behavior here proposed. It has also to be mentioned that the ultimate clear spherulites of PEN were negatively birefringent.

Discussion

Validity of the SAXS Analysis. In these studies of the multiple melting behavior of the three polymers,

Table 2. Calculations for the Systematic Melting of PEEK, PEN, and PET as a Function of the Temperature of Treatment[a,b]

polymer	T_c (°C)	$T_{heat\ up}$ (°C)	E_V (Å)	E_R (Å)	E_{RE} (Å)	L (Å)	ΔL (Å)	ΔL (%)	l (Å)
PEEK	280 (1 h)		7.5	6.3	5.4	132			38
		300	7.7	6.3	5.5	136	4	3	40
		335	7.8	6.6	5.6	167	31	27	43
PEN	210 (30 min)		9.5	11.0	6.8	133			40
		240	10.1	11.8	7.3	143	10	8	45
		260	11.9	11.8	8.6	198	55	49	65
PET	200 (30 min)		6.5	5.2	4.8	117			40
		220	7.2	5.8	5.2	130	13	11	45
		247	7.6	6.3	5.5	195	65	67	55

[a] Calculations based on the one-dimensional correlation function and independent calculation of transition layers. [b] L, long periodicity; l = lamellar thickness; E_V, transition layer Vonk/linear, E_R, transition layer Ruland/sigmoidal; E_{RE}, transition layer Ruland/sigmoidal-expanded.

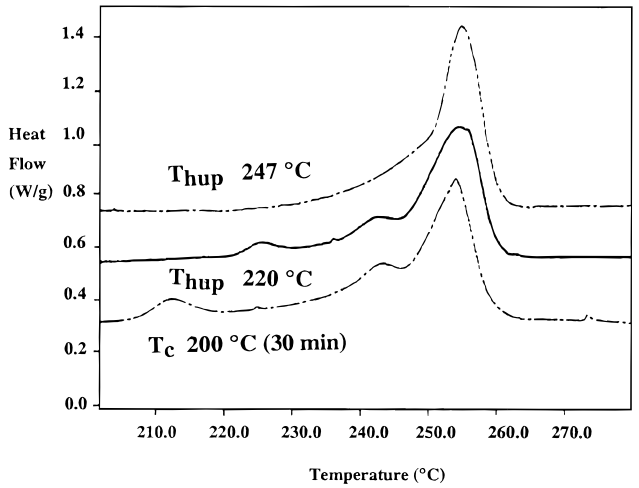

Figure 10. DSC traces of the systematic melting of PET. Crystallization from T_m = 300 °C, 3 min, and heating temperatures before quenching are shown.

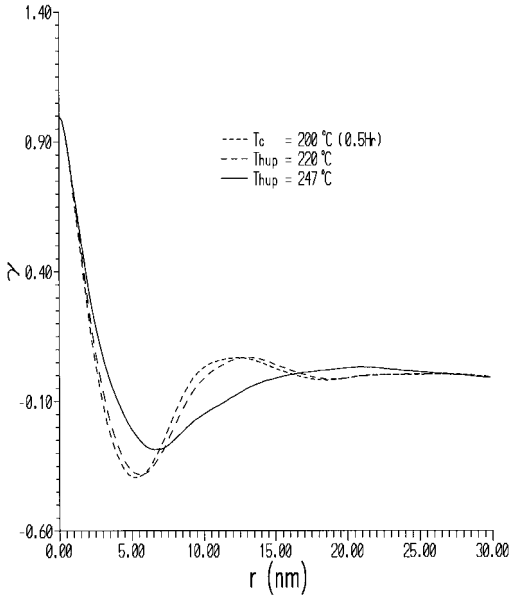

Figure 11. One-dimensional correlation function of PET under melting conditions. Crystallization and heating temperatures are shown.

SAXS yielded the most important complimentary results. However, it needs to be mentioned that the one-dimensional correlation function approach was originally designed for homogeneous (infinitely stacked) systems. One of our implied suggestions in this work, however, is that, at long crystallization times, spherulites in this family of macromolecules are inhomogeneously packed very probably by crystalline stacking due to secondary crystallization. In this form, for long

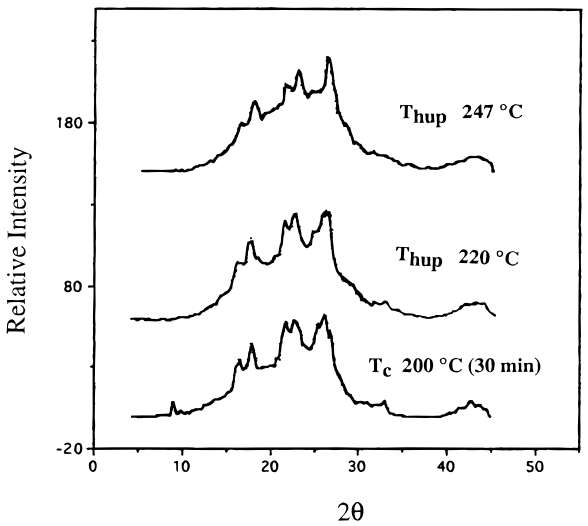

Figure 12. WAXD of systematic melting of PET. Crystallization and heating temperatures are shown.

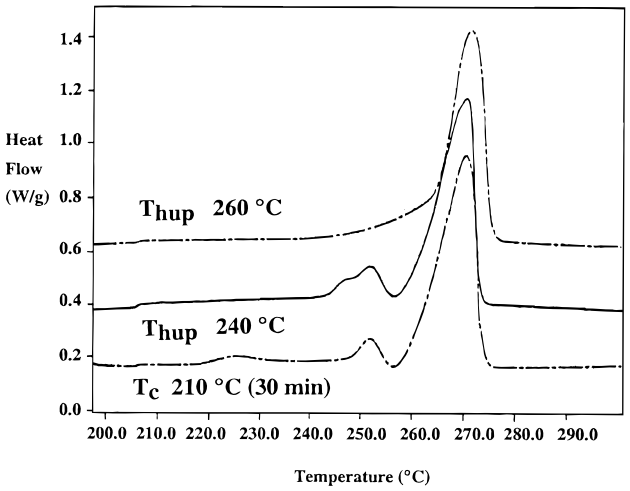

Figure 13. DSC traces of PEN crystallized at low times. Crystallization from T_m = 300 °C, 3 min, and heating temperatures before quenching are shown.

times of crystallization the amount of secondary crystallization would affect the shorter characteristic length and also the long spacing. Nevertheless, from the experimental point of view, we have chosen conditions of crystallization in such a way that secondary crystallinity is relatively low. This decreases (but does not eliminate) the probability of having inhomogeneous filling due to secondary crystallization. In support of these last arguments, there is a published study, in terms of stacking (at high crystallization times) for PET, by Santa Cruz et al.,[26] who from an analysis of the interface distribution function claimed that at high

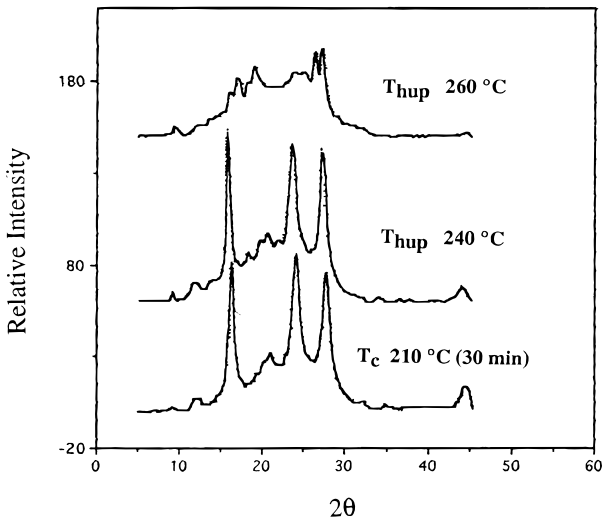

Figure 14. WAXD diffraction patterns for the systematic melting of PEN. Crystallization and heating temperatures are shown.

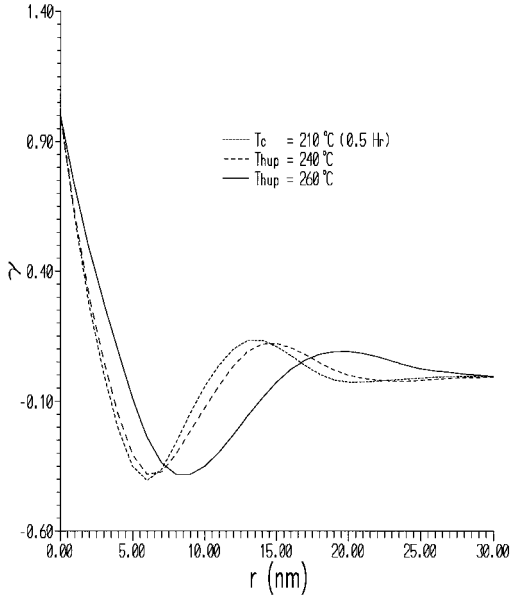

Figure 15. One-dimensional correlation function of the PEN systematic melting. Crystallization and heating temperatures are shown.

crystallization times (more than 1 h, i.e., well into the secondary crystallization range) PET spherulites were inhomogeneously filled with lamellar stacks. Specifically, they found six lamellae per stack under such conditions. The samples studied here were crystallized for a period of only 30 min, but interface distribution function models were also used in order to analyze our starting samples. The results shown in Figures 16−18 correspond to model calculations for each isothermal crystallization experiment, and in every case, it can be seen that infinite stacking (homogeneous filling) correlates better than finite stacking.

Crystallization Models. From evaluations of SAXS data, Wang et al.[27] determined that the long period, the lamellar thickness, and the crystallinity increased with the crystallization temperature when PEEK was isothermally crystallized. Their results were used to support the two-crystalline structures model, first proposed by Cheng et al.[9] and later on by Olley et al.[4] However, in situ SAXS melting experiments were not carried out, and the results were inferred from isothermal crystallization data.

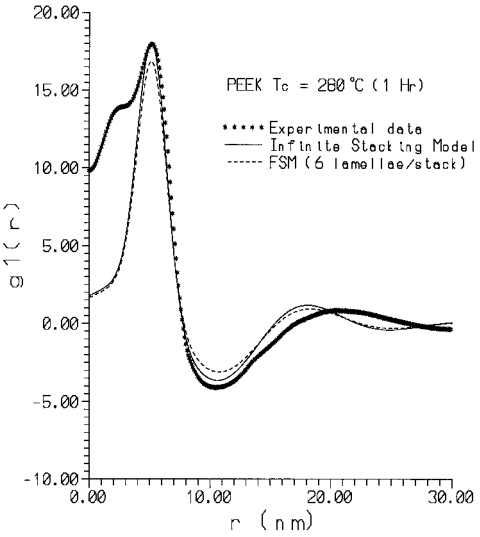

Figure 16. Model calculations for isothermally crystallized PEEK before melting.

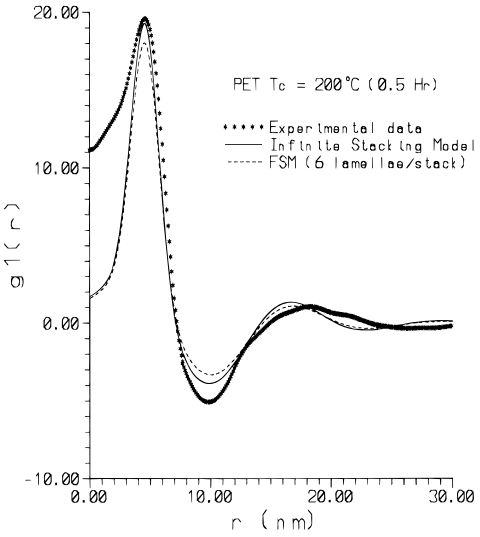

Figure 17. Model calculations for isothermally crystallized PET before melting.

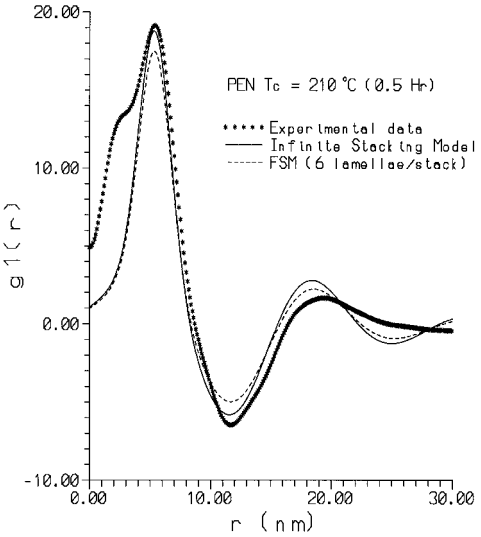

Figure 18. Model calculations for isothermally crystallized PEN before melting.

In the recent past, Hsiao et al.[5] carried out in situ SAXS heating measurements and also suggested that the lower melting endotherm observed immediately after the crystallization temperature was due to the

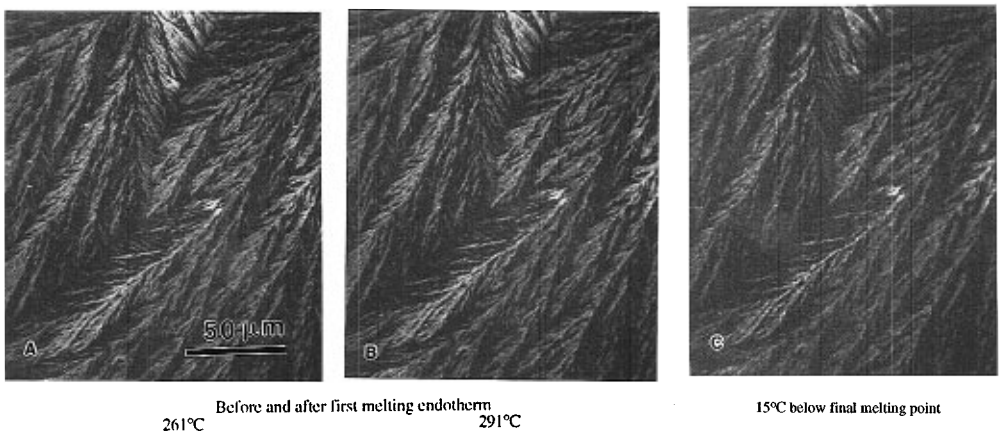

Figure 19. Melting of PEEK superstructures at T_c = 280 °C (T_m = 430 °C, 3 min).

melting of thin lamellae within the lamellar structures. They also concluded that the final melting endotherm would represent melting of thickened primary lamellae. This latter explanation is the most similar to the explanation given in this work; however, there are a number of differences which will be noted later.

Two types of long periodicity can be defined in terms of the one-dimensional correlation function. One corresponds to the position of the first maximum and it is related to the distance between the centers of gravity of two adjacent crystals. The other corresponds to double the position of the first minimum. The first minimum is associated with the distance between the center of gravity of one crystalline structure and the adjacent amorphous portion.[26] Both definitions are equivalent, however, when the concept of a possible "second" long periodicity is introduced,[5] in our opinion, it is simpler to use the first definition together with the hypothesis of a second intermediate lamellar structure present between two mother crystals. Using this approach, melting of the intermediate structure would increase the long period as shown in Figure 9. Melting of such intermediate crystalline structure would therefore explain the results at least in PEEK in agreement with the intermediate lamellar structures model. It does so for temperatures above the first melting endotherm and all the way up to temperatures near the final melting point.

Two main experimental facts are in disagreement with this latter model. First, melting of intermediate structures would lead to a well-defined two-phase system expected to show a "baseline" and also an increase in the intensity of the first maximum observed in the one-dimensional correlation function.[5,28] Second, optical observations of the process of melting are in disagreement with melting of an intermediate crystalline structure since a decrease of retardation on melting indicates a decrease of crystal thickness in the direction of view. If we consider that in PEEK spherulites the compounding lamellae are on-edge,[29] then a decrease of retardation on melting would indicate melting of structures on the edges of primary lamellae rather than between them. It has been shown[29] that in PEEK the dominant lamellae have widths close to their thicknesses and also that these lamellar structures are parallel and stand on their edges (along the plane of the lamellar thickness).

On the other hand, it should be noted that retardation results from a combination of thickness and birefringence ($r = t\Delta\eta$). On-edge lamellae would be highly birefringent because the *c*-axis polarizability is the largest of the three optical axes and is found in the plane of view. This is particularly the case in PEEK, where negative spherulites are present. We have assumed that birefringence ($\eta_2 - \eta_1$) remains constant in all cases, which would be a reasonable assumption as long as the lamellar thickness remains constant. Under these circumstances, there is also the possibility of generating flat-on material.[29] This would slightly and probably radially increase birefringence, and as a consequence, the retardation at constant (parent) lamellar thickness. The latter possibility is consistent with one of the characteristics that we observed, i.e., radial infilling. However, we observed rather strong changes in retardation along the direction of view at long crystallization times. They clearly followed the well-known Newton series as when there is an increase of retardation due to changes in thickness at constant birefringence, which then agrees with the idea that secondary crystalline structures are generated along the edges of mother crystals. The same kind of behavior was observed even if spherulites were positive as in the case of PET, i.e., where the *c* axis of the triclinic unit cell was perpendicular to the plane of view. Therefore, even though birefringence must be slightly changing, what is really affecting retardation is the evolution of crystal thickness along the direction of view.

Need for Another Model. An alternative way to explain the results would be to consider that primary lamellae in PEEK form certain secondary crystalline branches which overlap other primary crystalline lamellae and branches, giving rise to small regions of high concentration of crystals or of higher compounded thicknesses. Such regions would result in the development of high-order colors on crystallization which would gradually disappear on melting.

In summary, the first melting endotherm would be associated with melting of a portion of the last formed secondary crystals. In the case of PEEK a range of melting associated with thicker secondarily crystallized branches would come after the first melting endotherm and end at a temperature close to the final melting point. Finally, a third range of melting would be associated with the main crystals, which still might involve a relatively high amount of secondary thick branches and a much cleaner, but still broad, lamellar distribution as indicated in the one-dimensional correlation function and in agreement with optical observations.

One attempt to verify this hypothesis was made by crystallizing PEEK on glass substrates. The resulting superstructures are shown in the micrographs of Figure 19, where it can be corroborated that melting of secondary branches (probably nucleated from rejected mate-

rial) is the main characteristic of the process of melting of PEEK. The slight increase of lamellar thickness as melting proceeds, determined through SAXS, is easily explained in terms of melting of secondary branches and recrystallization of the melted material, which now can be trapped by the main crystal. The whole process finally gives place to thicker crystals with a higher melting point as discussed before. It has to be pointed out that, in the hypothesis presented, the phenomenon of melting and recrystallization is only partially involved. Krüger and Zachmann,[30] after studying the step crystallization and melting behavior of polyketones, concluded that the additional melting peaks were caused by melting of thin crystals rather than complete lamellar stacks. In addition, and as proposed here, they also supported the idea that at relatively low crystallization temperatures there can be partial melting followed by recrystallization.

Proposed Model. The interlamellar layer model[4,5,9,27] does not agree with the experimental facts of this work. Experimentally, at least, two inconsistencies have already been given. Conceptually, if the interlamellar space is too large, it will not generate enough stress to force secondary crystallization. In the opposite situation, too little space would generate the frozen-in morphology (random attachment and random packing at the interface) where space limitations[31] impede the formation of intermediate crystalline structures. Both conditions leave the interlamellar two-phase model in a position of requiring a near-to-ideal space distribution in order to develop the secondary layer.

As an alternative, consider the overall experimental "directions" of analyses of common morphological techniques. One example is the process of etching of surfaces and then replication and transmission electron microscopy (TEM) observations which would view along the direction in which an optical observation is made (normal to the plane of the sample surface). Disappearance of secondary crystalline structures would indicate that the material was in the middle of an average edge-on orientation (in the case of PEEK) of the main crystals (intermediate layer mechanism). On the other hand, SAXS analysis through the one-dimensional correlation function would "view" the lamellar stacks in such a way that, if secondary layers disappeared, the effect would be detected as an increase in the long periodicity (observed in the plot of the one-dimensional correlation function). This mechanism seems very logical, and probably these considerations led to the proposition of the interlayer model.

However, as mentioned before, several problems emerge, for example, from optical observations alone. As indicated in the case of PEEK, retardation (colors following Newton's series) in this work was observed to evolve increasingly along the direction of view under conditions of crystallization. The optical effect of introducing interlamellar crystalline material between edge-on lamellae (along the fold plane) would be a rather homogeneous, but very small increase in retardation, not as ubiquitous and strong as that observed experimentally.

It is possible that the rejected material, instead of violating the principle of packing at the interlamellar space, exits through coil deformation and development of protuberances along the lamellar edge. Such relatively ordered structures would act as primary nuclei for molecules that did not crystallize at the growth front but would be located close to the dominant lamellae.

In support of this hypothesis, a summary of experimental facts will be given now. Edge-on lamellar

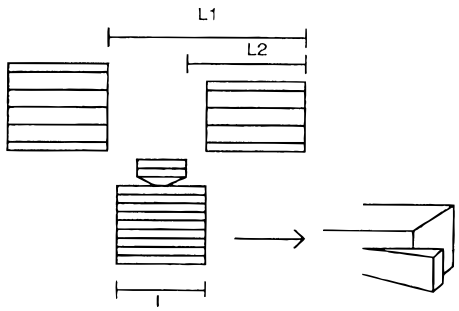

Figure 20. Negative edge-on branching model for isothermally crystallized PEEK and PEN.

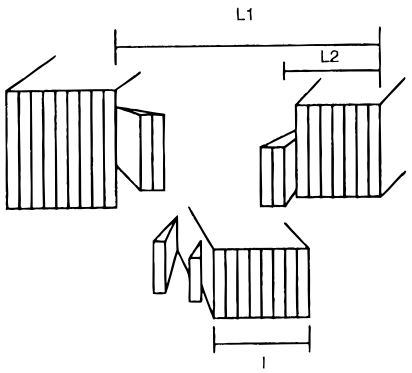

Figure 21. Positive edge-on branching model for PET.

structures have been seen in PEEK through surface analysis techniques such as scanning electron microscopy and TEM.[29] The optical effects observed here are related to changes in thickness in the direction of view. It should be recalled that there were less noticeable infilling effects disappearing at the second melting endotherm in PEEK than there were in PET. There was also a smaller decrease before melting in the long period of PEEK than in PET. Finally, we have to consider that after the Lorentz correction we are able to translate a spherical SAXS scattering system into a stacked one, i.e., one through which the one-dimensional correlation function "detects" morphological changes. Two models able to consider all such experimental characteristics are shown in Figures 20 and 21. The first model depicted in Figure 20 is one that would involve negative spherulites such as in PEEK. There would be two types of long periodicity and lamellar thicknesses as long as both primary and secondary crystals would be SAXS detectable. The second model is for positive spherulites such as those that occur in PET. It has the same characteristics as the first model but the main-chain axis is parallel to the direction of view but, even so, is able to explain the increase in retardation along the direction of view because the space is filled as a whole as the crystallization time increases.

In general terms, both models consist of random stacks with branches along the main-chain axis and so have relatively sharp boundaries, as is well-known in PET.[32,33] On further crystallization, the main lamellar structures compete with branches for crystallizable material as a function of the crystallization temperature. This, combined with the intrinsic rigidity of the chains preventing the development of grossly thicker crystalline structures, yields on average rather small lamellar thicknesses (in agreement with experimental facts).

The proposed models can also be explained in terms of surface free energies. If branches were developed on-edge then the fold surface free energy of the initial

lamellar structures (kinetic approach) would be very similar to that of the overall process of crystallization (thermodynamic approach). In support of this hypothesis, we have shown differences for PET of less than 3% between both values[34] ($\sigma_{eKI} = 22.4$ erg/cm^2; $\sigma_{eTH} = 25.3$ erg/cm^2). On the other hand, a strong change of the lateral surface free energy must be expected since proportionally it has to be the most affected parameter. As a rough reference, we can take the predicted Thomas–Stavely[35] average value of $\sigma = 18.98$ erg/cm^2 and the theoretical secondary nucleation theory $\sigma = 19.30$ erg/cm^2 and compare them with the experimental 45 erg/cm^2 for PET.[34,36]

A quantitative analysis of the one-dimensional correlation function is presented in Table 2. Numerical comparisons indicate that, as melting proceeds, PEEK and PET show very similar behavior but the different processes are present in different proportions. For example, the transition layer thickness remains almost constant during the process of melting. This is an indication that the lamellar structures do not melt through a surface melting mechanism or through a mechanism that involves the participation of the transition layer. These calculations also support the idea of melting of crystals in positions lateral to the dominant lamellae in PEEK and PET or one in which the thickness of the main lamellar structures remains relatively constant as melting proceeds. The process of melting of PEN is slightly different. The thickness of the transition layer remained again relatively constant, and there was an increase in the long period relatively proportional to the difference in chain stiffness between PEEK and PET. In this case, however, there was a larger increase in the lamellar thickness (higher recrystallization). Nonetheless, in general terms, the process of melting of PEN fits relatively well with the mechanism of stepwise melting.

Enhancement of secondary crystallization of PET as a function of molecular weight in order to determine the effect of rejected species from the main crystal is to be addressed in a future publication.[37]

Conclusions

The three high-temperature polymers PEEK, PET, and PEN first displayed, in appearance, different morphological features under isothermal crystallization and then melting. After a systematic analysis, it was concluded that considering the crystallization characteristics of each polymer, the melting behavior could be explained in terms of a triple process, taking as a reference, the DSC traces.

A general process of melting in terms of secondary branches, which might have been nucleated through rejected material and crystallized through nonprimarily crystallized polymer, is being proposed for the three polymers studied in this work. The process could be observed in spite of changes in morphology, changes in molecular orientation inside the lamellar crystals, and changes in crystalline structures. Therefore, it has the potential of being a general phenomenon for crystallization and melting of high-temperature semicrystalline polymers.

Acknowledgment. This research has been supported by the Polymers program of the National Science Foundation under Grants DMR-8719028 and DMR-9107675 and in part by the Division of Materials Sciences, U.S. Department of Energy under Contract DE-AC05-840R21400.

References and Notes

(1) Jaffe, M.; Wunderlich, B. *Kolloid-Z. Z. Polym.* **1967**, *216*, 203.
(2) Buckley, C. P.; Salem, D. R. *Polymer* **1987**, *28*, 69.
(3) Medellín-Rodríguez, F. J.; Phillips, P. J. *ANTEC-Tech. Pap.* **1991**, *37*, 893.
(4) Olley, R. H.; Bassett, D. C.; Blundell, D. J. *Polymer* **1986**, *27*, 344.
(5) Hsiao, B. S.; Gardner, K. H.; Wu, D. Q. *Polymer* **1993**, *34*, 3996.
(6) Lee, Y.; Porter, R. S. *Macromolecules* **1987**, *20*, 1336.
(7) Blundell, D. J.; Osborn, B. *Polymer* **1983**, *24*, 953.
(8) Blundell, D. J. *Polymer* **1987**, *28*, 2248.
(9) Cheng, S. Z. D.; Cao, M. Y.; Wunderlich, B. *Macromolecules* **1986**, *19*, 1868.
(10) Holdsworth, P. J.; Turner-Jones, A. *Polymer* **1971**, *12*, 195.
(11) Roberts, R. C. *J. Polym. Sci., Polym. Lett. Ed.* **1970**, *8*, 381.
(12) Roberts, R. C. *Polymer* **1969**, *10*, 117.
(13) Alfonso, G. C.; Pedemonte, E.; Ponzetti, L. *Polymer* **1979**, *20*, 104.
(14) Zhou, C.; Clough, S. B. *Polym. Eng. Sci.* **1988**, *28*, 65.
(15) Buchner, S.; Wiswe, D.; Zachmann, H. G. *Polymer* **1989**, *30*, 480.
(16) Wignall, G. D.; Lin, J. S.; Spooner, S. *J. Appl. Crystallogr.* **1990**, *23*, 241.
(17) Russell, T. P.; Lin, J. S.; Spooner, S.; Wignall, G. D. *J. Appl. Crystallogr.* **1988**, *21*, 629.
(18) Vonk, C. G.; Kortleve, G. *Kolloid-Z.* **1967**, *220*, 19.
(19) Koberstein, J. T.; Morra, B.; Stein, R. S. *J. Appl. Crystallogr.* **1980**, *13*, 34.
(20) Ruland, W. *J. Appl. Crystallogr.* **1971**, *4*, 70.
(21) Defoor, F. Ph.D. Dissertation, Katholieke Universiteit te Leuven, Leuven, Belgium, 1992.
(22) Siemann, U.; Ruland, W. *Colloid Polym. Sci.* **1982**, *260*, 999.
(23) Vonk, C. G. *J. Appl. Crystallogr.* **1973**, *6*, 81.
(24) Hsin-Lung, C.; Porter, R. S. *Polymer* **1993**, *34*, 4577.
(25) Medellin-Rodriguez, F. J. Ph.D. Dissertation, University of Tennessee, Knoxville, TN, 1993.
(26) Santa Cruz, C.; Stribeck, N.; Zachmann, H. G.; Balta Calleja, F. J. *Macromolecules* **1991**, *24*, 5980.
(27) Wang, J.; Alvarez, M.; Zhang, W.; Wu, Z.; Li, Y.; Chu, B. *Macromolecules* **1992**, *25*, 6943.
(28) Strobl, G. R.; Schneider, M. *J. Polym. Sci., Polym. Phys. Ed.* **1980**, *18*, 1343.
(29) Lovinger, A. J.; Davis, D. D. *J. Appl. Phys.* **1985**, *58*, 2843.
(30) Krüger, K.-N.; Zachmann, H. G. *Macromolecules* **1993**, *26*, 5202.
(31) Hoffman, J. D. *Polymer* **1983**, *24*, 3.
(32) Konrad, G.; Zachmann, H. G. *Colloid Polym. Sci.* **1971**, *247*, 851.
(33) Bornschlegl, E.; Bonart, R. *Colloid Polym. Sci.* **1980**, *258*, 319.
(34) Medellín-Rodríguez, F. J.; Phillips, P. J.; Lin, J. S., submitted to *Macromolecules*.
(35) Thomas, D. G.; Stavely, L. A. K. *J. Chem. Soc.* **1952**, 4569.
(36) Kaelble, D. H.; Cirlin, E. H. *J. Polym. Sci., A-2* **1971**, *9*, 363.
(37) Medellin-Rodriguez, F. J.; Phillips, P. J., to be published.

MA9511659